Nonlocal Polyakov–Nambu–Jona-Lasinio model with wave function renormalization at finite temperature and chemical potential

G. A. Contrera,[1,2] M. Orsaria,[2,3] and N. N. Scoccola[1,2,4]

[1]*Physics Department, Comisión Nacional de Energía Atómica, Av.Libertador 8250, 1429 Buenos Aires, Argentina*
[2]*CONICET, Rivadavia 1917, 1033 Buenos Aires, Argentina*
[3]*Gravitation, Astrophysics and Cosmology Group, FCAyG, UNLP, La Plata, Argentina*
[4]*Universidad Favaloro, Solís 453, 1078 Buenos Aires, Argentina*

(Received 25 June 2010; published 22 September 2010)

We study the phase diagram of strongly interacting matter in the framework of a nonlocal SU(2) chiral quark model which includes wave function renormalization and coupling to the Polyakov loop. Both nonlocal interactions based on the frequently used exponential form factor, and on fits to the quark mass and renormalization functions obtained in lattice calculations are considered. Special attention is paid to the determination of the critical points, both in the chiral limit and at finite quark mass. In particular, we study the position of the critical end point as well as the value of the associated critical exponents for different model parametrizations.

DOI: 10.1103/PhysRevD.82.054026 PACS numbers: 12.39.Ki, 11.30.Rd, 12.38.Mh

I. INTRODUCTION

At low temperatures and densities strongly interacting matter is believed to be in a phase in which chiral symmetry is broken and the quarks are confined. However, as the temperature (T) and/or the chemical potential (μ) increase some kind of transition to a chiral restored and/or deconfined phase is expected to happen. The detailed understanding of this phenomenon has become an issue of great interest in recent years, both theoretically and experimentally [1]. From the theoretical point of view, even if a significant progress has been made in the development of *ab initio* calculations such as lattice QCD [2–4], these are not yet able to provide a full understanding of the QCD phase diagram, due to the well-known difficulties of dealing with small current quark masses and finite chemical potentials. Thus, it is important to develop effective models that show consistency with lattice results and can be extrapolated into regions not accessible by lattice calculation techniques. Among them, the local Nambu-Jona-Lasinio (NJL) has been widely used to describe the behavior of strongly interacting matter at finite temperature and density [5]. In recent years an extension of the NJL model has been proposed in which the coupling of the quarks to the Polyakov loop is included. This so-called Polyakov–Nambu-Jona-Lasinio model [6–12] allows us to study the chiral and deconfinement transitions in a common framework. As an improvement over local models, the study of the phase diagram of chiral quark models that include nonlocal interactions [13] has been undertaken [14–16]. These theories can be viewed as nonlocal extensions of the NJL model. In fact, nonlocality arises naturally in the context of several successful approaches to low-energy quark dynamics as, for example, the instanton liquid model [17] and the Schwinger-Dyson resummation techniques [18]. Lattice QCD calculations [19,20] also indicate that quark interactions should act over a certain range in momentum space. In addition, several studies [21–24] have shown that nonlocal chiral quark models provide a satisfactory description of hadron properties at zero temperature and density. The aim of the present work is to extend previous studies of the chiral and deconfinement transitions in the framework of nonlocal chiral models with coupling to the Polyakov loop [25–27] by considering more general quark interactions. Following Refs. [28,29], we will adopt as the basic ingredient a reliable description of the $T = \mu = 0$ quark propagator as given from fundamental studies, such as lattice QCD. In this sense, it should be noticed that most of the finite T and/or μ calculations performed so far in the context of nonlocal chiral quark models have used exponential regulators and neglected the wave function renormalization in the quark propagator. Recent lattice QCD calculations suggest, however, that the wave function renormalization can be of the order of 30% (or even more) at zero momentum [19,20]. Moreover, these calculations also show that the quark masses tend to their asymptotic values in a rather soft way. Thus, it is important to perform a detailed study of the impact of the incorporation of these features on the predictions for the phase diagram and associated quantities. The Lagrangian we will use is the minimal extension which allows us to incorporate the full momentum dependence of the quark propagator, through its mass and wave function renormalization. Using such a model we will investigate the phase diagrams corresponding to different parametrizations, including one based on fits to the quark mass and renormalization functions obtained in lattice calculations, both in the chiral limit and for finite quark mass. The position of the critical points as well as the value of the associated critical exponents will be also studied.

This article is organized as follows. In Sec. II we provide a description of the model and its parametrizations. In

Sec. III we present and discuss the results obtained in the chiral limit, while those corresponding to finite values of the quark mass are given and analyzed in Sec. IV. In Sec. V we present a summary of our main results and conclusions. Finally, we include two appendices. In Appendix A we provide some details concerning the derivation of the Landau expansion associated with our model in the chiral limit, while in Appendix B we describe the formalism used to determine the position of the critical end point.

II. THE MODEL AND ITS PARAMETRIZATIONS

We consider a nonlocal SU(2) chiral quark model which includes quark couplings to the color gauge fields. The corresponding Euclidean effective action is given by

$$S_E = \int d^4x \Big\{ \bar{\psi}(x)(-i\gamma_\mu D_\mu + \hat{m})\psi(x) - \frac{G_S}{2}[j_a(x)j_a(x) - j_P(x)j_P(x)] + \mathcal{U}(\Phi[A(x)]) \Big\}, \quad (1)$$

where ψ is the $N_f = 2$ fermion doublet $\psi \equiv (u, d)^T$, and $\hat{m} = \mathrm{diag}(m_u, m_d)$ is the current quark mass matrix. In what follows we consider isospin symmetry, that is $m = m_u = m_d$. The fermion kinetic term includes a covariant derivative $D_\mu \equiv \partial_\mu - iA_\mu$, where A_μ are color gauge fields and the operator $\gamma_\mu \partial_\mu$ in Euclidean space is defined as $\vec{\gamma} \cdot \vec{\nabla} + \gamma_4 \frac{\partial}{\partial \tau}$, with $\gamma_4 = i\gamma_0$. The nonlocal currents $j_a(x)$, $j_P(x)$ are given by

$$j_a(x) = \int d^4z g(z) \bar{\psi}\Big(x + \frac{z}{2}\Big)\Gamma_a \psi\Big(x - \frac{z}{2}\Big), \qquad j_P(x) = \int d^4z f(z) \bar{\psi}\Big(x + \frac{z}{2}\Big)\frac{i\overleftrightarrow{\partial}}{2\kappa_p}\psi\Big(x - \frac{z}{2}\Big). \quad (2)$$

Here, $\Gamma_a = (\mathbb{1}, i\gamma_5\vec{\tau})$ and $u(x')\overleftrightarrow{\partial} v(x) = u(x')\partial_x v(x) - \partial_{x'}u(x')v(x)$. The functions $g(z)$ and $f(z)$ in Eq. (2), are nonlocal covariant form factors characterizing the corresponding interactions. The four standard quark currents $j_a(x)$ require the same $g(z)$ form factor to guarantee chiral invariance. The term $\frac{G}{2} j_P(x)j_P(x)$ is self-invariant under chiral transformations. The scalar-isoscalar component of the $j_a(x)$ current will generate the momentum dependent quark mass in the quark propagator, while the "momentum" current, $j_P(x)$, will be responsible for a momentum dependent wave function renormalization of this propagator. For convenience, we take the same coupling parameter, G_S, for both interaction terms. Note, however, that the relative strength between both interaction terms will be controlled by the mass parameter κ_p introduced in Eq. (2). In what follows it is convenient to Fourier transform $g(z)$ and $f(z)$ into momentum space. Note that Lorentz invariance implies that the Fourier transforms $g(p)$ and $f(p)$ can only be functions of p^2.

To proceed we perform a standard bosonization of the theory. Thus, we introduce the bosonic fields $\sigma_{1,2}(x)$ and $\pi_a(x)$, and integrate out the quark fields. In what follows, we work within the mean-field approximation (MFA), in which these bosonic fields are replaced by their vacuum expectation values $\sigma_{1,2}$ and $\pi_a = 0$. Since we are interested in studying the characteristics of the chiral phase transition we have to extend the so obtained bosonized effective action to finite temperature T and chemical potential μ. In the present work this is done by using the Matsubara formalism. Concerning the gluon fields we will assume that they provide a constant background color field $A_4 = iA_0 = ig\delta_{\mu 0}G_a^\mu \lambda^a/2$, where G_a^μ are the SU(3) color gauge fields. Then the traced Polyakov loop, which is taken as order parameter of confinement, is given by $\Phi = \frac{1}{3}\mathrm{Tr}\exp(i\phi/T)$, where $\phi = iA_0$. We will work in the so-called Polyakov gauge, in which the matrix ϕ is given a diagonal representation $\phi = \phi_3\lambda_3 + \phi_8\lambda_8$. This leaves only two independent variables, ϕ_3 and ϕ_8. At vanishing chemical potential, owing to the charge conjugation properties of the QCD Lagrangian, the mean-field traced Polyakov loop is expected to be a real quantity. Since ϕ_3 and ϕ_8 have to be real-valued [30], this condition implies $\phi_8 = 0$. In general, this need not be the case at finite μ [31–33]. As in, e.g., Refs. [10,30,34,35] we will assume that the potential $\mathcal{U}$ is such that the condition $\phi_8 = 0$ is well satisfied for the range of values of μ and T investigated here. The mean-field traced Polyakov loop is then given by $\Phi = \Phi^* = [1 + 2\cos(\phi_3/T)]/3$.

Within this framework the mean-field thermodynamical potential Ω^{MFA} is

$$\Omega^{\mathrm{MFA}} = -\frac{4T}{\pi^2}\sum_c \int_{p,n} \ln\Big[\frac{(\rho^c_{n,\vec{p}})^2 + M^2(\rho^c_{n,\vec{p}})}{Z^2(\rho^c_{n,\vec{p}})}\Big] + \frac{\sigma_1^2 + \kappa_p^2\sigma_2^2}{2G_S} + \mathcal{U}(\Phi, T). \quad (3)$$

Here, the shorthand notation $\int_{p,n} = \sum_n \int d^3\vec{p}/(2\pi)^3$ has been used, and $M(p)$ and $Z(p)$ are given by

$$M(p) = Z(p)[m + \sigma_1 g(p)], \qquad Z(p) = [1 - \sigma_2 f(p)]^{-1}. \quad (4)$$

In addition, we have defined

$$(\rho^c_{n,\vec{p}})^2 = [(2n+1)\pi T - i\mu + \phi_c]^2 + \vec{p}^2, \quad (5)$$

where the quantities ϕ_c are given by the relation $\phi = \mathrm{diag}(\phi_r, \phi_g, \phi_b)$. Namely, $\phi_c = c\phi_3$ with $c = 1, -1, 0$ for r, g, b, respectively.

To proceed we need to specify the explicit form of the Polyakov loop effective potential. Following Ref. [10] we consider

$$\mathcal{U}(\Phi, T) = \Big[-\frac{1}{2}a(T)\Phi^2 + b(T) \times \ln(1 - 6\Phi^2 + 8\Phi^3 - 3\Phi^4)\Big]T^4, \quad (6)$$

where the coefficients are parametrized as

$$a(T) = a_0 + a_1\left(\frac{T_0}{T}\right) + a_2\left(\frac{T_0}{T}\right)^2, \qquad b(T) = b_3\left(\frac{T_0}{T}\right)^3, \tag{7}$$

and the values of T_0, a_i, and b_3 are fitted to QCD lattice results.

$\Omega^{\rm MFA}$ turns out to be divergent and, thus, needs to be regularized. For this purpose we use the same prescription as in e.g. Ref. [15]. Namely,

$$\Omega^{\rm MFA}_{\rm reg} = \Omega^{\rm MFA} - \Omega^{\rm free} + \Omega^{\rm free}_{\rm reg} + \Omega_0, \tag{8}$$

where $\Omega^{\rm free}$ is obtained from Eq. (3) by setting $\sigma_1 = \sigma_2 = 0$ and $\Omega^{\rm free}_{\rm reg}$ is the regularized expression for the quark thermodynamical potential in the absence of fermion interactions,

$$\Omega^{\rm free}_{\rm reg} = -4T\int\frac{d^3\vec{p}}{(2\pi)^3}\sum_c\Big[\ln\Big(1+\exp\Big[-\frac{E_p-\mu+i\phi_c}{T}\Big]\Big) + \ln\Big(1+\exp\Big[-\frac{E_p+\mu+i\phi_c}{T}\Big]\Big)\Big], \tag{9}$$

with $E_p = \sqrt{\vec{p}^2 + m^2}$. Finally, note that in Eq. (8) we have included a constant Ω_0 which is fixed by the condition that $\Omega^{\rm MFA}_{\rm reg}$ vanishes at $T = \mu = 0$.

The mean-field values $\sigma_{1,2}$ and Φ at a given temperature or chemical potential, are obtained from a set of three coupled "gap" equations. This set of equations follows from the minimization of the regularized thermodynamical potential, that is

$$\frac{\partial\Omega^{\rm MFA}_{\rm reg}}{\partial\sigma_1} = \frac{\partial\Omega^{\rm MFA}_{\rm reg}}{\partial\sigma_2} = \frac{\partial\Omega^{\rm MFA}_{\rm reg}}{\partial\Phi} = 0. \tag{10}$$

Once the mean-field values are obtained, the behavior of other relevant quantities as a function of temperature and chemical potential can be determined. Here, we will be particularly interested in the chiral quark condensate $\langle\bar{q}q\rangle$ and the quark density ρ defined by

$$\langle\bar{q}q\rangle = \frac{\partial\Omega^{\rm MFA}_{\rm reg}}{\partial m}, \qquad \rho = -\frac{\partial\Omega^{\rm MFA}_{\rm reg}}{\partial\mu}, \tag{11}$$

as well as their corresponding susceptibilities, i.e., the chiral susceptibility $\chi_{\rm ch}$ and the quark number susceptibility χ_q, defined by

$$\chi_{\rm ch} = \frac{\partial\langle\bar{q}q\rangle}{\partial m}, \qquad \chi_q = \frac{\partial\rho}{\partial\mu}. \tag{12}$$

Finally, the specific heat C_V, is expressed as

$$C_V = -T\frac{\partial^2\Omega^{\rm MFA}_{\rm reg}}{\partial T^2}. \tag{13}$$

In order to fully specify the model under consideration we have to fix the model parameters as well as the form factors $g(q)$ and $f(q)$ which characterize the nonlocal interactions. Here, following Ref. [29] we consider two different types of functional dependencies for these form factors. The first one corresponds to the often used exponential forms,

$$g(q) = \exp(-q^2/\Lambda_0^2), \qquad f(q) = \exp(-q^2/\Lambda_1^2). \tag{14}$$

Note that the range (in momentum space) of the nonlocality in each channel is determined by the parameters Λ_0 and Λ_1, respectively. Fixing the current quark mass and chiral quark condensate at $T = \mu = 0$ to the reasonable values $m = 5.7$ MeV and $\langle\bar{q}q\rangle^{1/3} = 240$ MeV, the rest of the parameters are determined so as to reproduce the empirical values $f_\pi = 92.4$ MeV and $m_\pi = 139$ MeV, and $Z(0) = 0.7$ which is within the range of values suggested by recent lattice calculations [8,10]. In what follows this choice of model parameters and form factors will be referred to as parametrization Set B. The second type of form factor functional forms we consider is given by

$$g(q) = \frac{1+\alpha_z}{1+\alpha_z f_z(q)}\,\frac{\alpha_m f_m(q) - m\alpha_z f_z(q)}{\alpha_m - m\alpha_z}, \qquad f(q) = \frac{1+\alpha_z}{1+\alpha_z f_z(q)}\,f_z(q), \tag{15}$$

where

$$f_m(q) = [1 + (q^2/\Lambda_0^2)^{3/2}]^{-1}, \qquad f_z(q) = [1 + (q^2/\Lambda_1^2)]^{-5/2}. \tag{16}$$

As shown in Ref. [29], taking $m = 2.37$ MeV, $\alpha_m = 309$ MeV, $\alpha_z = -0.3$, $\Lambda_0 = 850$ MeV, and $\Lambda_1 = 1400$ MeV one can very well reproduce the momentum dependence of mass and renormalization functions obtained in lattice calculations as well as the physical values of m_π and f_π. In what follows this choice of model parameters and form factors will be referred to as parametrization Set C. Finally, in order to compare with previous studies where the wave function renormalization of the quark propagator has been ignored we consider a third parametrization (Set A). In such a case we take $Z(p) = 1$ [i.e. $f(p) = 0$] and an exponential parametrization for $g(p)$. Such a model corresponds to the "Scheme II" dis-

TABLE I. Set parameters and chiral condensates for $T = \mu = 0$.

		Set A	Set B	Set C
m_c	MeV	5.78	5.70	2.37
$G_s\Lambda_0^2$		20.650	32.030	20.818
Λ_0	MeV	752.20	814.42	850.00
κ_P	GeV	⋯	4.180	6.034
Λ_1	MeV	⋯	1034.5	1400.0
σ_1	MeV	424	529	442
σ_2		⋯	−0.43	−0.43
$-\langle q\bar{q}\rangle^{1/3}$	MeV	240	240	326

cussed in Ref. [24], from where we take the parameters corresponding to $\langle\bar{q}q\rangle^{1/3} = 240$ MeV. The values of the model parameters for each of the chosen parametrizations are summarized in Table I.

III. PHASE DIAGRAM IN THE CHIRAL LIMIT

In order to investigate the details of the phase diagram of the nonlocal models under study it is convenient to consider first the chiral limit $m = 0$. In this limit, general considerations imply that for sufficiently small values of chemical potential the chiral restoration transition is of second order with the transition temperature T_c decreasing as μ increases. At a certain value of $\mu = \mu_{\rm TCP}$ the transition becomes of first order. The point in the T-μ plane defined by $(T_{\rm TCP}, \mu_{\rm TCP})$ corresponds to the so-called "tricritical point" (TCP). For values of $\mu > \mu_{\rm TCP}$ the corresponding T_c continues to decrease until it reaches zero. This marks the end of the critical line, $\mu_c(0)$ being the corresponding critical chemical potential.

In the following we will concentrate on the second order transition region. In such a region, for a given chemical potential μ, the condensate $\langle\bar{q}q\rangle$ goes to zero when the temperature T approaches from below the critical value $T_c(\mu)$, above which $\langle\bar{q}q\rangle = 0$ and the chiral symmetry is restored. Thus, for $T \sim T_c(\mu)$ the thermodynamical potential admits an expansion in powers of the order parameter (in this case the quark condensate). As discussed in detail in Appendix A, in the chiral limit such expansion reads

$$\Omega_{\rm reg}^{\rm MFA} = \hat{\Omega}(\mu, T, \Phi_c, \sigma_{2c}) + A_c\langle\bar{q}q\rangle^2 + C_c\langle\bar{q}q\rangle^4 + \mathcal{O}(\langle\bar{q}q\rangle^6), \tag{17}$$

where the explicit expressions of $\hat{\Omega}$ and the coefficients A_c and C_c are given in Eqs. (A3) and (A11), respectively. Having established the Landau expansion in terms of the chiral condensate as a single independent variable, we can now analyze the characteristics of the phase transition following the standard textbook methods. For $C_c > 0$ the system undergoes a second order phase transition at a critical temperature T_c. For each value of μ, this critical temperature can be obtained by solving a set of coupled equations given by the condition $A_c = 0$ supplemented by Eqs. (A7). The values of $T_c(\mu)$ so obtained define a second order transition curve in the (T, μ) plane. As already mentioned, such a curve is a decreasing function of μ which starts at the critical temperature corresponding to the vanishing chemical potential $T_c(0)$ and ends up at the tricritical point. The position of TCP can be determined by imposing the additional condition $C_c = 0$. Namely, to obtain it one has to solve the set of coupled equations given by $A_c = C_c = 0$ together with Eqs. (A7).

To analyze the critical line beyond the TCP it is convenient to take T as an independent variable and consider $\mu_c(T)$. For $T < T_{\rm TCP}$, the transition turns out to be discontinuous (i.e. first order). In this case, for each value of T, there is a region of values of μ for which three different solutions of the full gap equations, Eqs. (10), exist. Two of them correspond to minima of the grand potential and the third one to a maximum. In the chiral limit considered in the present section, one of the minima has $\sigma_1 = 0$, while in the other σ_1 takes a finite (in general, non-negligible) value. Then, μ_c corresponds to the chemical potential at which the pressure associated with these two minima coincide.

The phase diagrams corresponding to our three parametrizations are displayed in Fig. 1 while the position of the characteristic points are given in Table II. In Fig. 1 the dotted line indicates the second order chiral transition line, the full line that of first order, and the dashed lines correspond to the deconfinement transition (the lower and upper lines correspond to $\Phi = 0.3$ and $\Phi = 0.5$, respectively). We see that as μ increases there appears a region where the system remains in its confined phase (signalled by Φ

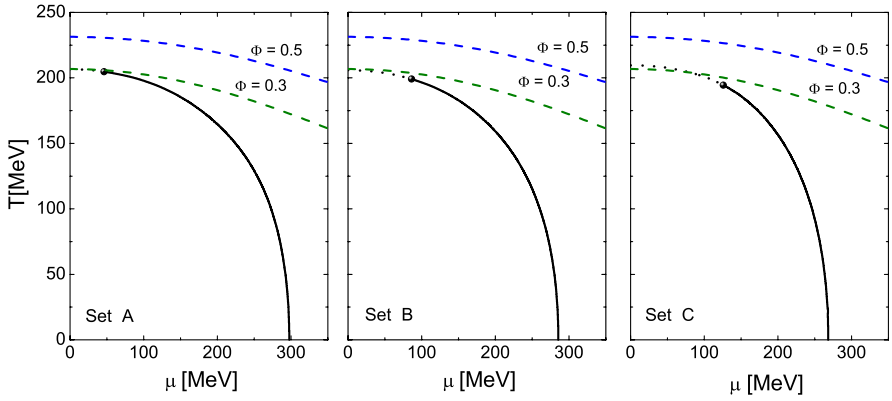

FIG. 1 (color online). Phase diagrams in the chiral limit for the three parametrizations considered. Set B and Set C include quark wave function renormalization while Set A does not. Set A and Set B correspond to exponential form factors while Set C corresponds to lattice motivated form factors. The dotted line corresponds to the second order chiral transition and the full line to that of first order one. The dashed lines correspond to the deconfinement transition (the lower and upper lines being for $\Phi = 0.3$ and $\Phi = 0.5$, respectively).

TABLE II. Position of some characteristic points of the phase diagrams in the chiral limit. All values are in MeV.

	Set A	Set B	Set C
$T_c(0)$	206.6	205.9	209.7
$\mu_{\rm TCP}$	46.2	86.1	125.7
$T_{\rm TCP}$	204.8	199.2	194.6
$\mu_c(0)$	297.6	285.5	268.2

smaller than $\simeq 0.3$) even though chiral symmetry has been restored. This corresponds to the recently proposed quarkyonic phase [36]. We observe that the general shape of the three diagrams is very similar with values of the critical temperatures at $\mu = 0$ differing by less than 4 MeV. In the case of the critical chemical potential at $T = 0$ the difference between the three sets is somewhat larger. Comparing the result of Set A with that of Set B we see that the inclusion of the wave function renormalization implies a decrease of about 10 MeV in the value of $\mu_c(0)$. The use of the softer form factors involved in the lattice inspired parametrization Set C leads to a further decrease of $\sim$10 MeV. The feature of the phase diagram that turns out to be most sensitive to the model parametrization is the position of the TCP. In fact, although the three values of $T_{\rm TCP}$ are in a range of about 10 MeV, the value of $\mu_{\rm TCP}$ increases by about a factor 2 when the wave function renormalization is included (i.e. when one goes from Set A to Set B) and by an extra factor $\sim 3/2$ when the lattice inspired parametrization Set C is used (i.e. when one goes from Set B to Set C).

As it is well known, in the region of the second order phase transition the behavior of several relevant thermodynamical quantities in the vicinity of the phase transition is determined by the critical exponents. In the case of the chiral and quark number susceptibilities, $\chi_{\rm ch}$ and χ_q respectively, and the specific heat C_V, they are usually defined by

$$\chi_{\rm ch} = |h - h_c|^{-\gamma_{\rm ch}}, \qquad \chi_q = |h - h_c|^{-\gamma_q}, \qquad C_V = |h - h_c|^{-\alpha}, \tag{18}$$

where $|h - h_c|$ is the distance to the critical point in the (μ, T) plane. Note that in the chiral limit only trajectories approaching the transition from the chirally broken phase are relevant. In the present case, given the Landau expansion obtained above, one expects to have the usual mean-field exponents. For trajectories which are not asymptotically tangential to the critical line they are

$$\gamma_{\rm ch} = 1, \qquad \gamma_q = 0, \qquad \alpha = 0, \tag{19}$$

for all points except for the TCP where

$$\gamma_{\rm ch} = 1, \qquad \gamma_q = 1/2, \qquad \alpha = 1/2. \tag{20}$$

As a test of consistency we have determined them numerically by studying the asymptotic behavior of the corresponding quantities for our three sets of parameters. As an example of a typical result of such studies we show in the left panel of Fig. 2 the behavior of $\chi_{\rm ch}$ for Set C as we approach an arbitrary point in second order transition line, i.e., a point *different* from the TCP, at constant μ (for definiteness we consider $\mu = 10$ MeV). The right panel in Fig. 2 displays the results of a equivalent study for $\mu = \mu_{\rm TCP}$. The values of the critical exponents extracted from this type of analysis for Set C are given in Table III. Very similar results are found for Set A and Set B. We see that in all cases the numerically obtained values are in very good agreement with the mean-field ones given above.

We finish this section by clarifying the role played by the Polyakov loop in enhancing the critical temperature at a given value of μ, at least in the region where the transition is of second order. For simplicity we consider the parametrization Set A where there is no wave function renormal-

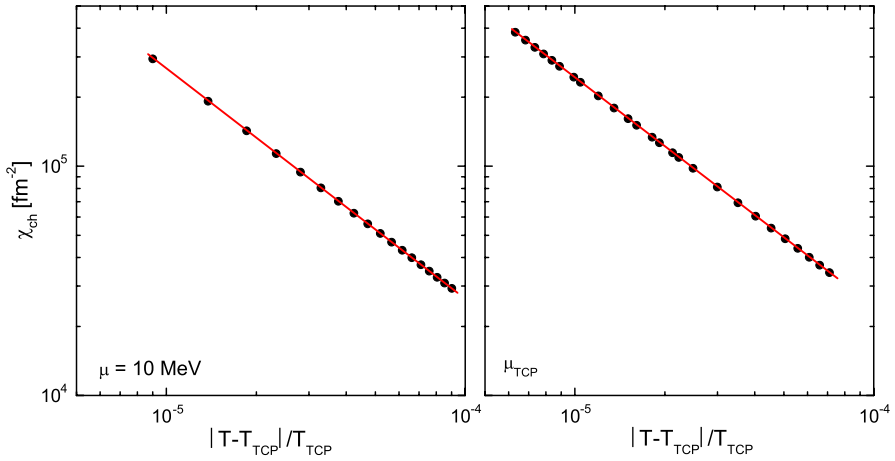

FIG. 2 (color online). Dependence of the chiral susceptibility $\chi_{\rm ch}$ as a function of T for constant μ in the vicinity of an arbitrary point (taken to correspond to $\mu = 10$ MeV) in the 2nd order transition line (left panel) and the TCP (right panel) in the chiral limit for parametrization Set C.

TABLE III. Critical exponents in the chiral limit for Set C.

		$\gamma_{\rm ch}$	γ_q	α
Point in 2nd order	$\mu \to$	1.00(1)	0.00(1)	0.00(1)
	$T \uparrow$	1.00(1)	0.00(1)	0.00(1)
critical line	MF exponent	1	0	0
TCP	$\mu \to$	1.00(1)	0.51(1)	0.50(1)
	$T \uparrow$	1.00(1)	0.51(1)	0.50(1)
	MF exponent	1	1/2	1/2

ization. The condition $A_c = 0$ implies $1/8G = S_{21}$ (see Appendix A). However, following similar steps as those described in Appendix B of Ref. [15], it is possible to show that for T, $\mu \ll \Lambda_0$ one has

$$S_{21} \simeq S_{21}^{\rm app} = \frac{3}{8\pi^2}\left(\frac{\Lambda_0^2}{4} - \left[\frac{\pi^2}{3} - \frac{2}{3}\left(\arccos\left[\frac{3\Phi - 1}{2}\right]\right)^2\right]T^2 - \mu^2\right). \tag{21}$$

In fact, we have checked numerically that in the relevant regions $T \leq 210$ MeV and $\mu \leq 50$ MeV, Eq. (21) is verified with an accuracy higher than 15% for $\Phi \leq 0.3$. Therefore, the condition $A_c = 0$ leads to

$$T_c(\mu) \simeq \frac{T_c^{(\rm pq)}(\mu)}{\sqrt{1 - \frac{2}{\pi^2}(\arccos[\frac{3\Phi_c - 1}{2}])^2}}, \tag{22}$$

where

$$T_c^{(\rm pq)}(\mu) = \frac{\sqrt{3}\Lambda_0}{2\pi}\sqrt{1 - \frac{4\pi^2}{3G_S\Lambda_0^2} - \frac{4\mu^2}{\Lambda_0^2}}. \tag{23}$$

$T_c^{(\rm pq)}(\mu)$ provides a good approximation to the critical temperature corresponding to the pure quark (pq) nonlocal model, i.e., the model with no coupling to the Polyakov loop (PL), for the exponential regulator considered in parametrization Set A (see Ref. [15] for details). Of course, in the presence of PL-quark interactions the value of Φ_c in Eq. (22) has to be obtained by simultaneously solving the corresponding gap equation, i.e., the second equation in Eq. (A7) in the present case. However, we clearly see that for any value of $\Phi_c < 1$ we have $T_c(\mu) > T_c^{\rm pq}(\mu)$. For example, at $\mu = 0$ one typically has $\Phi_c \simeq 0.2$ which implies $T_c(0)/T_c^{\rm pq}(0) \approx 1.66$. Since for the parametrization Set A we have $T_c^{\rm pq}(0) = 126$ MeV for the pure quark nonlocal model in the chiral limit, we see that the coupling to the PL is expected to raise this value up to $T_c \sim 209$ MeV which is in very good agreement with the numerically found value listed in Table II. As it is clear from Eqs. (22) and (23) a similar enhancement of the critical temperature can be obtained at (low) finite μ. On the other hand, it should be noticed that in order to apply the present type of analysis to relate the values of $\mu_c(T)$ predicted in models with and without PL one must have a common range of temperatures for which the transition is of second order. However, for the parametrizations considered here this is not possible since they always lead to $T_{\rm TCP} > T_c^{\rm pq}(0)$. For example, from Table II we see that Set A leads to $T_{\rm TCP} = 204.8$ MeV to be compared with the value $T_c^{\rm pq}(0) = 126$ MeV quoted above.

IV. PHASE DIAGRAM FOR FINITE QUARK MASS

We start by analyzing the behavior of some mean-field quantities as functions of T and μ. Since the results obtained for our three different parametrizations are qualitatively quite similar we only present explicitly those corresponding to the parametrization Set C. They are given in Fig. 3 where we plot σ_1, σ_2, and Φ as functions of T for some representative values of the chemical potential. The left panel of Fig. 3 shows that at $\mu = 0$ there is a certain value of T at which σ_1 drops rapidly, signalling the existence of a chiral symmetry restoration crossover transition. At basically the same temperature the Polyakov loop Φ increases which can be interpreted as the onset of the deconfinement transition. As μ increases there is a certain value of $\mu = \mu_{\rm CEP}$ above which the transition starts to be discontinuous. At this precise chemical potential the transition is of second order. This situation is illustrated in the

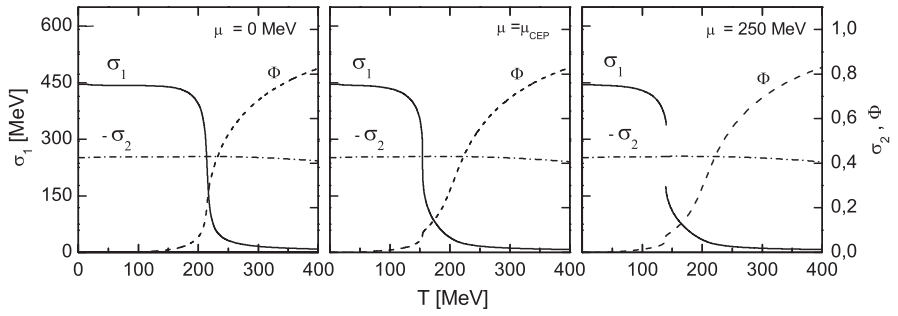

FIG. 3. Mean fields σ_1, σ_2, and Φ as functions of T at three representative values of chemical potentials for parametrization Set C. Note that the scale to the left corresponds to σ_1 while that to the right corresponds to σ_2 and Φ. Since σ_2 turns out to be negative we plot $-\sigma_2$.

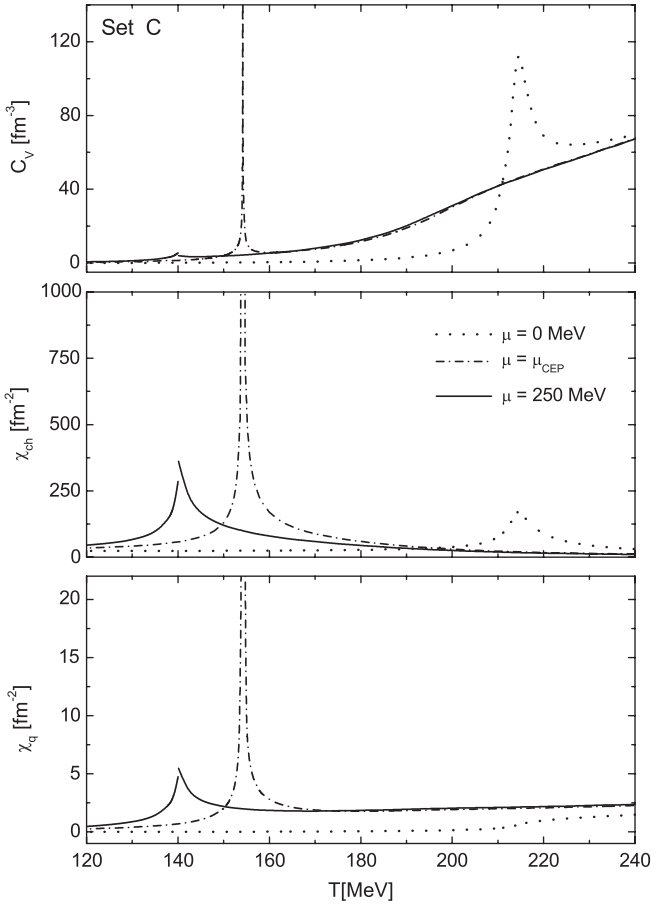

FIG. 4. Behavior of the specific heat C_V, the chiral susceptibility $\chi_{\rm ch}$, and the quark number susceptibility χ_q as functions of T at three representative values of chemical potentials for parametrization Set C.

central panel of Fig. 3. The corresponding values $(T_{\rm CEP}, \mu_{\rm CEP})$ define the position of the so-called "critical end point" (CEP) which, as explained in Appendix B, can be found by solving a system of equations formed by the gap equations, Eqs. (10), supplemented by two additional equations of the following type: (B3) and (B4). As displayed in the right panel of Fig. 3, for $\mu > \mu_{\rm CEP}$ the transition becomes discontinuous, i.e., of first order. Finally, for chemical potentials above $\mu_c(T=0) \simeq 310$ MeV the system is in the chirally restored phase for all values of the temperature. It is important to note that although σ_2 appears to be rather constant in Fig. 3, at higher values of T it does go to zero as expected.

The different nature of the chiral transition in each of the three regions of Fig. 3 is even more clearly observed in the behavior of the corresponding response functions. In Fig. 4 we display the specific heat C_V as well as the chiral and quark number susceptibilities, $\chi_{\rm ch}$ and χ_q, as a function of the temperature for parametrization Set C and the three different values of μ used in Fig. 3. The dotted line corresponds to $\mu = 0$. We observe that all the response functions show a rather broad peak of finite height at basically the same value of T. Such a value of T corresponds to the temperature at which the crossover transition occurs. The dashed-dotted line corresponds to $\mu = \mu_{\rm CEP}$ which indicates that all the response functions display a sharp and narrow divergent peak. Such a behavior signals the second order nature of the chiral transition at the CEP. Finally, the full line corresponds to $\mu > \mu_{\rm CEP}$. In all cases we observe a discontinuity in the response functions which indicates that the associated transition is of first order.

The phase diagrams corresponding to our three different parametrizations are given in Fig. 5. Here the dotted line represents the line of crossover chiral transition while the full line represents that of first order. The dashed lines are associated to the deconfinement transition (the lower and upper lines correspond to $\Phi = 0.3$ and $\Phi = 0.5$, respectively). The position of the most relevant points in the phase diagrams are tabulated in Table IV. As in the chiral case, we observe that the main difference appears in the

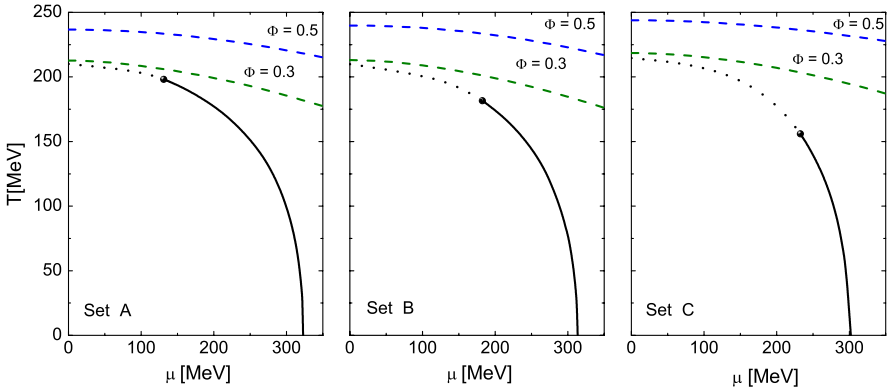

FIG. 5 (color online). Phase diagrams for the three parametrizations considered. Set B and Set C include quark wave function renormalization while Set A does not. Set A and Set B correspond to exponential form factors while Set C corresponds to lattice motivated form factors. The dotted line corresponds to the line of crossover chiral transition and the full line to that of first order chiral transition. The dashed lines correspond to the deconfinement transition (the lower and upper lines being for $\Phi = 0.3$ and $\Phi = 0.5$, respectively).

TABLE IV. Position of some characteristic points of the phase diagrams for finite quark mass. All values are in MeV.

	Set A	Set B	Set C
$T_c(0)$	210.0	209.8	214.5
$\mu_{\rm CEP}$	132.5	182.3	234.8
$T_{\rm CEP}$	197.8	181.6	154.2
$\mu_c(0)$	321.5	311.6	298.1

position of the point at which the first order transition line ends. Comparing the results of Set A and Set B we see that the main effect of the wave function renormalization term is to shift the location of the CEP towards lower values of T and higher values of μ. Concerning the lattice motivated parametrization Set C we observe that it leads to even lower values of $T_{\rm CEP}$ and higher values of $\mu_{\rm CEP}$. Comparing with the results obtained in the chiral limit we note that the variation of $T_{\rm CEP}$ between different sets is larger in this case. Moreover, considering each parametrization separately we observe that while the effect of introducing a finite quark mass on the values of the $T_c(0)$ and $\mu_c(0)$ is quite small (approximately $+5$ MeV and $+30$ MeV, respectively), the position of the CEP is much more sensitive to the value of the current quark mass m, especially in the case of parametrization Set C. This is clearly seen in Fig. 6 where we plot $T_{\rm CEP}$ and $\mu_{\rm CEP}$ as a function of m. In all the cases we note a sharp decrease (increase) of $T_{\rm CEP}$ ($\mu_{\rm CEP}$) for low values of m. In the case of the exponential parametrization Set A and Set B, at $m \sim 4$ MeV this variation tends to disappear and the position of the CEP remains rather stable up to the maximum value of m we have considered. On the other hand, for the lattice motivated parametrization the situation is somewhat different. In fact, the variation is rather large for basically all the values of m considered. In particular we see that, after the initial sharp decrease, at about 4 MeV the value of $T_{\rm CEP}$ starts to increase in a rather pronounced way. It is interesting to note that the behavior of the position of the CEP as a function of m close to $m = 0$ (i.e. close to the TCP) can be analytically investigated [37]. General arguments imply that

$$\Delta T_{\rm CEP} = T_{\rm CEP}(m) - T_{\rm TCP} = -cm^{2/5} + \mathcal{O}(m^{4/5}),$$
$$\Delta \mu_{\rm CEP} = \mu_{\rm CEP}(m) - \mu_{\rm TCP} = +dm^{2/5} + \mathcal{O}(m^{4/5}), \quad (24)$$

where c and d are definite positive constants. To verify that our results do satisfy these relations we have numerically studied in detail the variation of $T_{\rm CEP}$ and $\mu_{\rm CEP}$ as a function of m close to the chiral limit. Results for the parametrization Set C are shown in Fig. 7 where the power-law behavior of both $\Delta T_{\rm CEP}$ and $\Delta \mu_{\rm CEP}$ is clearly seen as a straight line in the corresponding log-log plot. Performing a linear fit we obtain that the slope of both straight lines is 0.40 ± 0.01 in very good agreement with the exponents in Eq. (24).

Finally, we consider the behavior of the response functions close to the CEP. As already mentioned, the chiral phase transition at this point is of second order. Thus, a critical behavior with critical exponents defined as in Eq. (18) is expected. Within the approximations used in this work these exponents should take the mean-field values $\gamma_{\rm ch} = \gamma_q = \alpha = 2/3$ when one approaches the CEP using trajectories which are not asymptotically parallel to the first order transition line. As mentioned in Sec. III, these exponents can be numerically obtained by analyzing the asymptotic behavior of the response functions close to the critical point. In Fig. 8 we show a typical result of this type of numerical study. There, we display a log-log plot of the specific heat C_V corresponding to the parametrization Set C as a function of the relative temperature departure $|T - T_{\rm CEP}|/T_{\rm CEP}$ for trajectories that approach the CEP at constant $\mu = \mu_{\rm CEP}$ both from below (i.e. $T < T_{\rm CEP}$) and from above (i.e. $T > T_{\rm CEP}$). We observe that a single straight line behavior is obtained up to relative departure as large as 10^{-3} after which nonlinear effects start to show

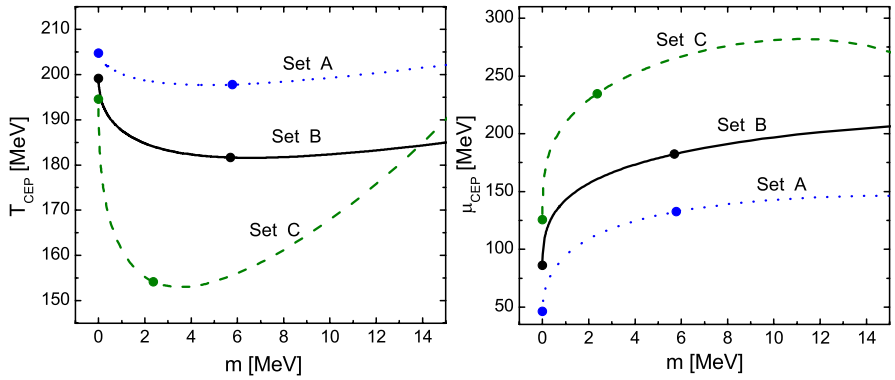

FIG. 6 (color online). Position of the CEP in the (T, μ) plane as a function of the current quark mass m for the three model parametrizations used in this work. The left panel displays the dependence of $T_{\rm CEP}$ while the right panel displays that of $\mu_{\rm CEP}$. Values corresponding to the chiral limit $m = 0$ and to the "physical" current quark masses given in Table I for each parameter set are indicated by fat dots.

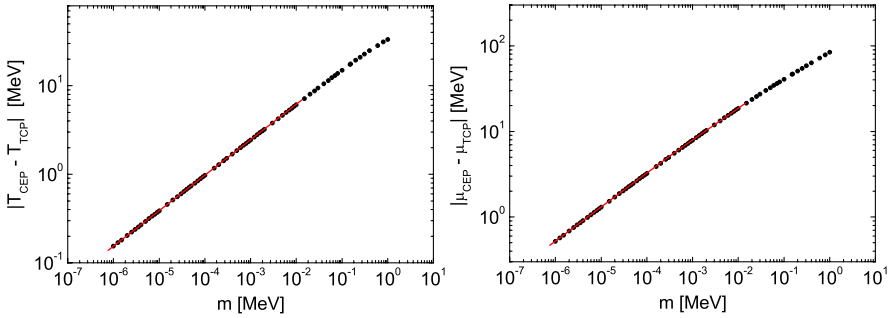

FIG. 7 (color online). Position of the CEP in the (T, μ) plane as a function of the current quark mass m close to the chiral limit for parametrization Set C.

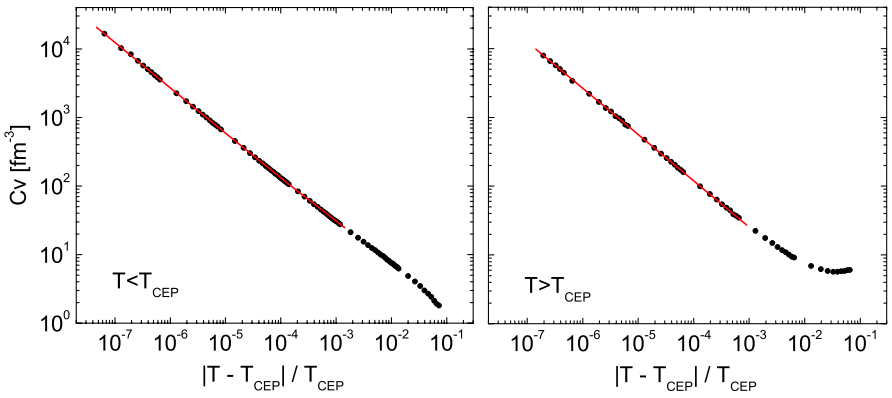

FIG. 8 (color online). Dependence of the specific heat C_V as a function of T for constant μ in the vicinity of the CEP for parametrization Set C. The left panel displays the dependence as one approaches the CEP from below while the right panel displays the one when the approach is done from above.

up. This result is particularly interesting since there have been claims [37,38] that in some cases there might be a "two straight lines" behavior, namely, that two different critical exponents are needed in order to describe the critical behavior of the C_V close to the CEP. In fact, this feature has been interpreted as an influence of the TCP critical properties on the CEP ones. As displayed in Fig. 8 no sign of this type of effect is found in our case. Results similar to those presented in this figure have been obtained for the chiral and quark number susceptibilities. The corresponding values of the critical exponents for different kind of trajectories are listed in Table V. Note that in all cases the agreement with the mean-field values of the exponents is very good. The same type of results has been found for the other two parametrizations, i.e., the exponential parametrizations Set A and Set B. It should be stressed that in order to obtain numerically the critical exponents with a good accuracy it is important to know the position of the CEP with very good precision. We have checked that even an error of 0.5 MeV in T_{CEP} and/or μ_{CEP} translates into an important uncertainty in the critical exponents. In this sense, the method for the determination of the CEP discussed in Appendix B is of great help.

TABLE V. Critical exponents at the CEP for Set C.

	γ_{ch}	γ_q	α
$\mu \rightarrow$	0.67(1)	0.67(1)	0.66(1)
$\mu \leftarrow$	0.66(1)	0.66(1)	0.67(1)
$T \uparrow$	0.67(1)	0.67(1)	0.66(2)
$T \downarrow$	0.66(1)	0.66(1)	0.67(1)
MF exponent	2/3	2/3	2/3

V. SUMMARY AND CONCLUSIONS

In this work we have studied the behavior of strongly interacting matter at the finite temperature and chemical potential using a nonlocal chiral quark model which includes wave function renormalization and coupling to the Polyakov loop. This type of model can be understood as a nonlocal extension of the local Polyakov–Nambu-Jona-Lasinio model, and represents a step toward a more realistic modeling of the QCD interactions that could allow a simultaneous description of the deconfinement and chiral phase transition. The nonlocal interactions have been described by considering not only the frequently used exponential form factors, but also a parametrization based on fits to the quark mass and renormalization functions obtained in lattice calculations. In this framework, we have studied the corresponding phase diagrams and associated

quantities, both in the chiral limit and at finite values of the current quark mass, paying particular attention to the accurate determination of the critical points. In fact, in both cases we have been able to obtain a set of coupled equations for the position of the corresponding critical point, i.e., the TCP in the chiral limit and the CEP for finite quark mass. Our numerical results indicate that some of the features of the phase diagrams are not very much dependent on the different parametrizations we used. For example, for the finite quark mass the critical temperatures at $\mu = 0$ are within the range 210–215 MeV, while the critical chemical potentials at $T = 0$ are in the range of 298–322 MeV. On the other hand, the position of the critical point turns out to be very sensitive to both the parametrization and the value of the current quark mass m. Comparing the results corresponding to the exponential parametrization with and without quark wave function renormalization we find that the main effect of the presence of this term is to shift the location of the CEP towards lower values of T and higher values μ. Concerning the lattice motivated parametrization we observe that it leads to even lower values of $T_{\rm CEP}$ and higher values of $\mu_{\rm CEP}$. As for the dependence on m we have verified that for small values of m (i.e. close to the TCP) the position of the CEP displays in all cases a power-law behavior, as expected. For the exponential parametrizations at $m \sim 4$ MeV this initial variation tends to disappear and the position of the CEP remains rather stable up to the maximum value of m we have considered. On the other hand, for the lattice motivated parametrization the situation is somewhat different. In fact, the dependence on m is rather strong for basically all the values considered. In particular, after an initial sharp decrease, at $m \sim 4$ MeV the value of $T_{\rm CEP}$ starts to increase in a rather pronounced way. Finally, we have analyzed numerically the critical behavior around the TCP and the CEP determining the critical exponents associated with the chiral and quark number susceptibilities as well as the heat capacity. In all cases, we find that the obtained exponents agree with their predicted mean-field values to a rather good degree of accuracy. In particular, no influence of the TCP properties on the CEP critical exponents has been found.

ACKNOWLEDGMENTS

We would like to acknowledge useful discussions with D. Gomez Dumm. This work was supported by CONICET (Argentina) Grant No. PIP 00682 and by ANPCyT (Argentina) Grant No. PICT07 03-00818.

APPENDIX A: DERIVATION OF THE LANDAU EXPANSION

To derive the Landau expansion, Eq. (17), we start by assuming that the chemical potential μ is such that, in the chiral limit, the chiral condensate vanishes at a critical temperature $T_c(\mu)$. Since in that situation the mean-field value σ_1 also vanishes, for $T \sim T_c(\mu)$ it is possible to perform a double expansion of $\Omega_{\rm reg}^{\rm MFA}$, Eq. (8), in powers of σ_1 and m. We obtain

$$\begin{aligned}\Omega_{\rm reg}^{\rm MFA}&(\mu, T, \Phi, \sigma_2, \sigma_1)\\ &= \hat{\Omega}(\mu, T, \Phi, \sigma_2) + 4\left[\frac{1}{8G} - S_{21}(\mu, T, \Phi, \sigma_2)\right]\sigma_1^2\\ &\quad + 2S_{42}(\mu, T, \Phi, \sigma_2)\sigma_1^4 - 8m\sigma_1[S_{11}(\mu, T, \Phi, \sigma_2)\\ &\quad - S_{32}(\mu, T, \Phi, \sigma_2)\sigma_1^2] + \mathcal{O}(\sigma_1^6, m\sigma_1^5, m^2\sigma_1^2),\end{aligned} \tag{A1}$$

where

$$S_{jk}(\mu, T, \Phi, \sigma_2) = \sum_c \int_{p,n} g^j(\rho^c_{n,\vec{p}})\left(\frac{Z^2(\rho^c_{n,\vec{p}})}{(\rho^c_{n,\vec{p}})^2}\right)^k, \tag{A2}$$

and $\hat{\Omega}(\mu, T, \Phi, \sigma_2)$ is the MFA thermodynamical potential in the chiral limit for vanishing σ_1. Namely,

$$\begin{aligned}\hat{\Omega}(\mu, T, \Phi, \sigma_2) = \frac{8T}{\pi^2}\sum_c \int_{p,n} \ln Z(\rho^c_{n,\vec{p}}) + \frac{\kappa_p^2\sigma_2^2}{2G_S}\\ + \mathcal{U}(\Phi, T) + \Omega_{\rm reg}^{\rm free} + \Omega_0.\end{aligned} \tag{A3}$$

Using Eq. (11) the corresponding expression for the chiral condensate can be readily obtained. In the chiral limit we get

$$\begin{aligned}\langle\bar{q}q\rangle &= 8\sigma_1[S_{11}(\mu, T, \Phi, \sigma_2) - S_{32}(\mu, T, \Phi, \sigma_2)\sigma_1^2]\\ &\quad + \mathcal{O}(\sigma_1^5).\end{aligned} \tag{A4}$$

Inverting this equation and replacing in Eq. (A1) we finally get

$$\begin{aligned}\Omega_{\rm reg}^{\rm MFA}&(\mu, T, \Phi, \sigma_2, \langle\bar{q}q\rangle)\\ &= \hat{\Omega}(\mu, T, \Phi, \sigma_2) + A(\mu, T, \Phi, \sigma_2)\langle\bar{q}q\rangle^2\\ &\quad + C(\mu, T, \Phi, \sigma_2)\langle\bar{q}q\rangle^4 + \mathcal{O}(\langle\bar{q}q\rangle^6).\end{aligned} \tag{A5}$$

Here, the coefficients A and C are given by

$$\begin{aligned}A(\mu, T, \Phi, \sigma_2) &= \frac{1}{4S_{11}^2(T, \mu, \Phi, \sigma_2)}\\ &\quad \times\left[\frac{1}{8G} - S_{21}(T, \mu, \Phi, \sigma_2)\right],\\ C(\mu, T, \Phi, \sigma_2) &= \frac{S_{42}(T, \mu, \Phi, \sigma_2)}{128S_{11}^4(T, \mu, \Phi, \sigma_2)}\\ &\quad - \frac{S_{32}(T, \mu, \Phi, \sigma_2)}{32S_{11}^5(T, \mu, \Phi, \sigma_2)}\\ &\quad \times\left[\frac{1}{8G} - S_{21}(T, \mu, \Phi, \sigma_2)\right].\end{aligned} \tag{A6}$$

The expansion Eq. (A5) looks very similar to Eq. (15) of Ref. [15] where nonlocal models in the absence of wave function renormalization and coupling to the Polyakov loop were analyzed. In principle, following similar ideas,

explicit equations for the second order transition line as well as the position of the TCP point might be determined. However, the fact that in the present case the coefficients A and C depend on the mean-field values σ_2 and Φ introduces further complications. In fact, slightly below T_c (for a given value of μ) the nonvanishing value of the condensate induces departures of (Φ, σ_2) from the critical values $(\Phi_c, \sigma_{2,c})$ obtained as solutions of the set of equations

$$\left.\frac{\partial\hat{\Omega}(\mu, T_c(\mu), \Phi, \sigma_2)}{\partial\sigma_2}\right|_{\Phi_c,\sigma_{2,c}} = \left.\frac{\partial\hat{\Omega}(\mu, T_c(\mu), \Phi, \sigma_2)}{\partial\Phi}\right|_{\Phi_c,\sigma_{2,c}} = 0. \tag{A7}$$

Those departures can be obtained using the gap equations resulting from Eq. (A5). To quadratic order in the condensate, we obtain

$$\sigma_2 = \sigma_{2,c} - \frac{(\partial^2_{\Phi\Phi}\hat{\Omega}_c)(\partial_{\sigma_2}A_c) - (\partial^2_{\Phi\sigma_2}\hat{\Omega}_c)(\partial_\Phi A_c)}{(\partial^2_{\Phi\Phi}\hat{\Omega}_c)(\partial^2_{\sigma_2\sigma_2}\hat{\Omega}_c) - (\partial^2_{\Phi\sigma_2}\hat{\Omega}_c)^2}\langle\bar{q}q\rangle^2,$$
$$\Phi = \Phi_c - \frac{(\partial^2_{\sigma_2\sigma_2}\hat{\Omega}_c)(\partial_\Phi A_c) - (\partial^2_{\Phi\sigma_2}\hat{\Omega}_c)(\partial_{\sigma_2}A_c)}{(\partial^2_{\Phi\Phi}\hat{\Omega}_c)(\partial^2_{\sigma_2\sigma_2}\hat{\Omega}_c) - (\partial^2_{\Phi\sigma_2}\hat{\Omega}_c)^2}\langle\bar{q}q\rangle^2, \tag{A8}$$

where a compact notation has been used to denote the derivatives of $\hat{\Omega}$ and A evaluated at T_c. In this notation we have, for example,

$$\left.\frac{\partial\hat{\Omega}(\mu, T_c(\mu), \Phi, \sigma_2)}{\partial\bar{\Phi}}\right|_{\Phi_c,\sigma_{2,c}} = \partial_\Phi\hat{\Omega}_c, \qquad \left.\frac{\partial A(\mu, T_c(\mu), \Phi, \sigma_2)}{\partial\sigma_2}\right|_{\Phi_c,\sigma_{2,c}} = \partial_{\sigma_2}A_c. \tag{A9}$$

Using Eqs. (A8) we can now obtain the leading corrections to A, C, and $\hat{\Omega}$ induced by the nonvanishing value of the condensate. Replacing the corresponding results in Eq. (A5), and grouping in powers of $\langle\bar{q}q\rangle$ we finally obtain Eq. (17). Namely,

$$\Omega^{\mathrm{MFA}}_{\mathrm{reg}} = \hat{\Omega}(\mu, T, \Phi_c, \sigma_{2,c}) + A_c\langle\bar{q}q\rangle^2 + C_c\langle\bar{q}q\rangle^4 + \mathcal{O}(\langle\bar{q}q\rangle^6), \tag{A10}$$

where

$$A_c = A(\mu, T_c(\mu), \Phi_c, \sigma_{2,c}),$$
$$C_c = C(\mu, T_c(\mu), \Phi_c, \sigma_{2,c}) - \frac{(\partial^2_{\sigma_2\sigma_2}\hat{\Omega}_c)(\partial_\Phi A_c)^2 + (\partial^2_{\Phi\Phi}\hat{\Omega}_c)(\partial_{\sigma_2}A_c)^2 - 2(\partial^2_{\Phi\sigma_2}\hat{\Omega}_c)(\partial_{\sigma_2}A_c)(\partial_{\sigma_2}A_c)}{[2(\partial^2_{\Phi\Phi}\hat{\Omega}_c)(\partial^2_{\sigma_2\sigma_2}\hat{\Omega}_c) - (\partial^2_{\Phi\sigma_2}\hat{\Omega}_c)^2]}. \tag{A11}$$

APPENDIX B: FORMALISM TO DETERMINE THE POSITION OF THE CEP

As discussed in Ref. [37], in the case in which the grand potential Ω depends on one single variational parameter, a set of equations that allows us to determine the position of the CEP can be obtained. This set is formed by the corresponding gap equation supplemented with the two equations that result from demanding that the second and third total derivatives of the grand potential with respect to the parameter also vanish. Physically, this corresponds to determining the values of (T, μ) for which the grand potential around its minimum is as flat as possible. The purpose of this appendix is to give some details of the formalism needed to generalize this idea to the case in which the grand potential depends on more than one variational parameter. In order to keep the derivation as general as possible we will assume here that the grand potential depends on N variational parameters $\xi_1, \xi_2, \ldots, \xi_N$. For convenience, in what follows, we will distinguish ξ_1 from the rest (note that there is no loss of generality in this choice since the ordering of the parameters is completely arbitrary), and introduce the Latin index $j = 2, \ldots, N$. Then, in a compact notation, the set of gap equations reads

$$\frac{\partial\Omega}{\partial\xi_1} = 0, \tag{B1}$$

$$\frac{\partial\Omega}{\partial\xi_j} = 0. \tag{B2}$$

The basic idea is now to consider the variational parameters ξ_j as functions of ξ_1 with the corresponding functional dependence determined by the solutions of the $N-1$ gap equations, Eqs. (B2). The total set of $N+2$ equations needed to determine the CEP is then obtained by supplementing these $N-1$ equations with those resulting from demanding that the first, second, and third *total* derivatives of the grand potential with respect to ξ_1 vanish. The first of these equations turns out to be, of course, the gap equation Eq. (B1). The other two are

$$\frac{\partial^2\Omega}{\partial\xi_1^2} + 2\frac{\partial^2\Omega}{\partial\xi_1\partial\xi_j}\xi_j' + \frac{\partial^2\Omega}{\partial\xi_j\partial\xi_k}\xi_j'\xi_k' = 0, \tag{B3}$$

$$\frac{\partial^3\Omega}{\partial\xi_1^3} + 3\frac{\partial^3\Omega}{\partial\xi_1^2\partial\xi_j}\xi_j' + 3\frac{\partial^3\Omega}{\partial\xi_1\partial\xi_j\partial\xi_k}\xi_j'\xi_k' + 3\frac{\partial^3\Omega}{\partial\xi_j\partial\xi_k\partial\xi_l}\xi_j'\xi_k'\xi_l' + 3\frac{\partial^2\Omega}{\partial\xi_j\partial\xi_k}\xi_j'\xi_k'' + 3\frac{\partial^2\Omega}{\partial\xi_1\partial\xi_j}\xi_j'' = 0. \quad \text{(B4)}$$

Here, and in what follows, the sum over repeated Latin indexes $k, j, l = 2, \ldots, N$ is understood. Note that in obtaining these equation some terms have been dropped assuming that the gap equations, Eqs. (B1) and (B2), are simultaneously satisfied. In Eqs. (B3) and (B4), ξ_j', ξ_j'', etc., denote the derivatives of the corresponding parameters with respect to ξ_1. They can be conveniently expressed in terms of partial derivatives of the grand potential by solving the two sets of linear equations resulting from taking the first and second total derivatives of both sides of the gap equations, Eq. (B2). We obtain

$$\xi_j' = -(C^{-1})_{jk}\frac{\partial^2\Omega}{\partial\xi_1\partial\xi_k}, \quad \text{(B5)}$$

$$\xi_j'' = -(C^{-1})_{jk}\left[\frac{\partial^3\Omega}{\partial\xi_1^2\partial\xi_k} + 2\frac{\partial^3\Omega}{\partial\xi_1\partial\xi_j\partial\xi_k}\xi_k' + \frac{\partial^3\Omega}{\partial\xi_j\partial\xi_k\partial\xi_l}\xi_k'\xi_l'\right], \quad \text{(B6)}$$

where

$$C_{jk} = \frac{\partial^2\Omega}{\partial\xi_j\partial\xi_k}. \quad \text{(B7)}$$

Therefore, once the explicit form of the grand potential Ω in terms of the variational parameters is known, all the derivatives appearing in the set of equations, Eqs. (B1)–(B4), can be analytically determined. Then, the numerical solution of this set of equations allows us to determine the values of (T, μ) corresponding to the CEP as well as the corresponding values of the variational parameters $\xi_1, \xi_2, \ldots, \xi_N$.

Turning to the model discussed in the present work, we note that for the parametrizations Set B and Set C we have three variational parameters. We chose to identify them as $\xi_1 = \sigma_1$, $\xi_2 = \sigma_2$, and $\xi_3 = \Phi$. Then, the set of five equations needed to determine the CEP is formed by Eqs. (10) supplemented by the two equations that result from performing the corresponding identifications in Eqs. (B3)–(B7). In the case of parametrization Set A the situation is somewhat simpler since there are only two variational parameters ($\xi_1 = \sigma_1$ and $\xi_2 = \Phi$) and, hence, four equations are required to determine the CEP.

[1] See, e.g., D. H. Rischke, Prog. Part. Nucl. Phys. **52**, 197 (2004); P. Jacobs and X. N. Wang, Prog. Part. Nucl. Phys. **54**, 443 (2005); K. Fukushima and T. Hatsuda, arXiv:1005.4814.

[2] C. R. Allton *et al.*, Phys. Rev. D **68**, 014507 (2003); **71**, 054508 (2005).

[3] Z. Fodor and S. D. Katz, J. High Energy Phys. 04 (2004) 050; Y. Aoki, Z. Fodor, S. D. Katz, and K. K. Szabo, J. High Energy Phys. 01 (2006) 089.

[4] F. Karsch and E. Laermann, in *Quark Gluon Plasma III* edited by R. C. Hwa and X. N. Wang (World Scientific, Singapore, 2004).

[5] U. Vogl and W. Weise, Prog. Part. Nucl. Phys. **27**, 195 (1991); S. Klevansky, Rev. Mod. Phys. **64**, 649 (1992); T. Hatsuda and T. Kunihiro, Phys. Rep. **247**, 221 (1994); M. Buballa, Phys. Rep. **407**, 205 (2005).

[6] P. N. Meisinger and M. C. Ogilvie, Phys. Lett. B **379**, 163 (1996).

[7] K. Fukushima, Phys. Lett. B **591**, 277 (2004).

[8] E. Megias, E. Ruiz Arriola, and L. L. Salcedo, Phys. Rev. D **74**, 065005 (2006).

[9] C. Ratti, M. A. Thaler, and W. Weise, Phys. Rev. D **73**, 014019 (2006).

[10] S. Roessner, C. Ratti, and W. Weise, Phys. Rev. D **75**, 034007 (2007).

[11] S. Mukherjee, M. G. Mustafa, and R. Ray, Phys. Rev. D **75**, 094015 (2007).

[12] C. Sasaki, B. Friman, and K. Redlich, Phys. Rev. D **75**, 074013 (2007).

[13] G. Ripka, *Quarks Bound by Chiral Fields* (Oxford University Press, Oxford, 1997).

[14] I. General, D. Gomez Dumm, and N. N. Scoccola, Phys. Lett. B **506**, 267 (2001); D. Gomez Dumm and N. N. Scoccola, Phys. Rev. D **65**, 074021 (2002).

[15] D. Gomez Dumm and N. N. Scoccola, Phys. Rev. C **72**, 014909 (2005).

[16] R. S. Duhau, A. G. Grunfeld, and N. N. Scoccola, Phys. Rev. D **70**, 074026 (2004); D. Gomez Dumm, D. B. Blaschke, A. G. Grunfeld, and N. N. Scoccola, Phys. Rev. D **73**, 114019 (2006).

[17] T. Schafer and E. V. Shuryak, Rev. Mod. Phys. **70**, 323 (1998).

[18] C. D. Roberts and A. G. Williams, Prog. Part. Nucl. Phys. **33**, 477 (1994); C. D. Roberts and S. M. Schmidt, Prog. Part. Nucl. Phys. **45**, S1 (2000).

[19] P. O. Bowman, U. M. Heller, and A. G. Williams, Phys. Rev. D **66**, 014505 (2002); P. O. Bowman, U. M. Heller, D. B. Leinweber, and A. G. Williams, Nucl. Phys. B, Proc. Suppl. **119**, 323 (2003); M. B. Parappilly, P. O. Bowman, U. M. Heller, D. B. Leinweber, A. G. Williams, and J. B.

Zhang, Phys. Rev. D **73**, 054504 (2006).
[20] S. Furui and H. Nakajima, Phys. Rev. D **73**, 074503 (2006).
[21] R. D. Bowler and M. C. Birse, Nucl. Phys. **A582**, 655 (1995); R. S. Plant and M. C. Birse, Nucl. Phys. **A628**, 607 (1998).
[22] W. Broniowski, B. Golli, and G. Ripka, Nucl. Phys. **A703**, 667 (2002); A. H. Rezaeian, N. R. Walet, and M. C. Birse, Phys. Rev. C **70**, 065203 (2004).
[23] A. Scarpettini, D. Gomez Dumm, and N. N. Scoccola, Phys. Rev. D **69**, 114018 (2004).
[24] D. Gomez Dumm, A. G. Grunfeld, and N. N. Scoccola, Phys. Rev. D **74**, 054026 (2006).
[25] G. A. Contrera, D. Gomez Dumm, and N. N. Scoccola, Phys. Lett. B **661**, 113 (2008); Phys. Rev. D **81**, 054005 (2010).
[26] D. Blaschke, M. Buballa, A. E. Radzhabov, and M. K. Volkov, Yad. Fiz. **71**, 2012 (2008) [Phys. At. Nucl.**71**, 1981 (2008)].
[27] T. Hell, S. Roessner, M. Cristoforetti, and W. Weise, Phys. Rev. D **79**, 014022 (2009); T. Hell, S. Roessner, M. Cristoforetti, and W. Weise, Phys. Rev. D **81**, 074034 (2010).
[28] S. Noguera, Int. J. Mod. Phys. E **16**, 97 (2007); S. Noguera and V. Vento, Eur. Phys. J. A **28**, 227 (2006).
[29] S. Noguera and N. N. Scoccola, Phys. Rev. D **78**, 114002 (2008).
[30] S. Roessner, T. Hell, C. Ratti, and W. Weise, Nucl. Phys. **A814**, 118 (2008).
[31] H.-T. Elze, D. E. Miller, and K. Redlich, Phys. Rev. D **35**, 748 (1987).
[32] A. Dumitru, R. D. Pisarski, and D. Zschiesche, Phys. Rev. D **72**, 065008 (2005).
[33] K. Fukushima and Y. Hidaka, Phys. Rev. D **75**, 036002 (2007).
[34] H. Abuki, M. Ciminale, R. Gatto, G. Nardulli, and M. Ruggieri, Phys. Rev. D **77**, 074018 (2008); H. Abuki, R. Anglani, R. Gatto, G. Nardulli, and M. Ruggieri, Phys. Rev. D **78**, 034034 (2008).
[35] D. Gomez Dumm, D. B. Blaschke, A. G. Grunfeld, and N. N. Scoccola, Phys. Rev. D **78**, 114021 (2008).
[36] L. McLerran and R. D. Pisarski, Nucl. Phys. **A796**, 83 (2007); L. McLerran, K. Redlich, and C. Sasaki, Nucl. Phys. **A824**, 86 (2009).
[37] Y. Hatta and T. Ikeda, Phys. Rev. D **67**, 014028 (2003).
[38] P. Costa, C. A. de Sousa, M. C. Ruivo, and Yu. L. Kalinovsky Phys. Lett. B **647**, 431 (2007); P. Costa, C. A. de Sousa, M. C. Ruivo, and H. Hansen, Europhys. Lett. **86**, 31001 (2009).